Atmos. Chem. Phys. Discuss., https://doi.org/10.5194/acp-2019-20
Manuscript under review for journal Atmos. Chem. Phys.
Discussion started: 18 February 2019

Atmospheric Chemistry and Physics Discussions

Secondary organic aerosol formation from OH-initiated oxidation of *m*-xylene: effects of relative humidity on yield and chemical composition

Qun Zhang[1,2], Yongfu Xu[1,2,*], Long Jia[1,2]

[1]State Key Laboratory of Atmospheric Boundary Layer Physics and Atmospheric Chemistry, Institute of Atmospheric Physics, Chinese Academy of Sciences, Beijing 100029, China,
[2]Department of Atmospheric Chemistry and Environmental Sciences, College of Earth Sciences, University of Chinese Academy of Sciences, Beijing 100049, China

Correspondence to: Yongfu Xu (xyf@mail.iap.ac.cn)

Abstract. The effect of relative humidity (RH) on the secondary organic aerosol (SOA) formation from the photooxidation of *m*-xylene initiated by OH radicals in the absence of seed particles was investigated in a smog chamber. The SOA yields were determined based on the particle mass concentrations measured with a scanning mobility particle sizer (SMPS) and reacted *m*-xylene concentrations measured with a gas chromatograph-mass spectrometer (GC-MS). The SOA components were analysed using Fourier transform infrared spectrometer (FTIR) and ultrahigh performance liquid chromatograph-electrospray ionization-high-resolution mass spectrometer (UPLC-ESI-HRMS). A significant discrepancy was observed in SOA mass concentration and yield variation with the RH conditions. The SOA yield is 13.8% and 0.8% at low RH (13.7%) and high RH (79.1%), respectively, with the difference being over an order of magnitude. The relative increase of C-O-C at high RH from the FTIR analysis of functional groups indicates that the oligomers from carbonyl compounds cannot well explain the suppression of SOA yield. Highly oxygenated molecules (HOMs) were observed to be suppressed in the HRMS spectra. The chemical mechanism for explaining the RH effects on SOA formation from *m*-xylene-OH system is proposed based on the analysis of both FTIR and HRMS measurements as well as Master Chemical Mechanism (MCM) simulations. The reduced SOA at high RH is mainly ascribed to the less formation of oligomers and the suppression of RO_2 autoxidation. As a result, high RH can obstruct the oligomerization and autoxidation that contribute to the SOA formation.

1 Introduction

Secondary organic aerosol (SOA) is a significant component of atmospheric fine particulate matter in the troposphere (Hallquist et al., 2009; Spracklen et al., 2011; Huang et al., 2014), leading to serious concerns as it has a significant influence on the air quality, oxidative capacity of the troposphere, global climate change and human health (Jacobson et al., 2000; Hansen and Sato, 2001; Kanakidou et al., 2005; Zhang et al., 2014). In a previous study from a global model simulation, it has been found that SOA represents a large fraction, approximately 80% of the total organic aerosol sources (Spracklen et al., 2011).

Atmos. Chem. Phys. Discuss., https://doi.org/10.5194/acp-2019-20
Manuscript under review for journal Atmos. Chem. Phys.
Discussion started: 18 February 2019

Atmospheric Chemistry and Physics Discussions

The formation of SOA in the atmosphere is principally via the oxidation of volatile organic compounds (VOCs) by common atmospheric oxidants such as O_3, OH and NO_3 radicals (Seinfeld and Pandis, 2016). Aromatic compounds mainly from anthropogenic source, including solvent usage, oil-fired vehicles and industrial emissions, contribute 20-30% to the total VOCs in urban atmosphere, which play a significant role in the formation of ozone and SOA in the urban troposphere (Forstner et al., 1997; Odum et al., 1997; Calvert et al., 2002; Bloss et al., 2005; Offenberg et al., 2007; Ding et al., 2012; Zhao et al., 2017). Amongst aromatics, *m*-xylene is significant, of which mean concentration together with *p*-xylene in daytime was determined up to 140.8 μg m^{-3} in atmosphere of urban areas in developing countries (Khoder, 2007).

The oxidation of aromatics in the troposphere is mainly initiated through OH radicals, which is affected by many chemical and physical factors. The concentrations of oxidant species, VOCs and NO_x concentrations, as well as the ratio of VOCs to NO_x (Ge et al., 2017c) determine the main chemical mechanism. Light intensity (Warren et al., 2008), temperature (Qi et al., 2010) and relative humidity (RH) are the most significant physical parameters that affect the chemical process. RH governs the water concentration in the gas phase and the liquid water content (LWC) in the particle phase. Water plays a significant role that can serve as reactant, product and solvent to directly participate in chemistry (Finlayson-Pitts and Pitts Jr., 2000) and indirectly affect the reaction environment such as acidity of particles (Jang et al., 2002).

Investigations of RH effects on aromatics SOA have conducted in many previous works. In the presence of NO_x, it was observed that RH significantly enhanced the yield of SOA from benzene, toluene, ethylbenzene and xylenes photooxidation, which was explained by a higher formation of HONO, particle water, aqueous radical reactions and the hydration from glyoxal (Healy et al., 2009; Kamens et al., 2011; Zhou et al., 2011; Jia and Xu, 2014, 2018; Wang et al., 2016). Meanwhile, under low NO_x condition that no NO_x were introduced artificially and photolysis of H_2O_2 was as an OH radical source, it has been observed that deliquesced seed contributed to the enhancement of SOA yield from toluene (Faust et al., 2017; Liu et al., 2018). However, under low NO_x level, it has been found that, in the study on toluene SOA formation, moderate RH level (48%) leads to a lower SOA yield than low RH level (17-18%), while in the presence of NO_x, RH effects were opposite (Cao and Jang, 2010). In a most recent study on SOA formation of toluene (Hinks et al., 2018), high RH led to a much lower SOA yield than low RH under low NO_x level, which is attributed to condensation reactions that remove water, leading to the less oligomerization at high RH. In a study on chemical oxidative potential of SOA (Tuet et al., 2017) under low NO_x conditions, it was observed that the mass concentration of SOA from *m*-xylene irradiation under the dry condition was much larger than that under the humid condition, whereas the study did not focus on the RH effect on *m*-xylene SOA formation. These demonstrate that the RH effects on aromatics SOA yields, especially *m*-xylene, have not been fully understood and the RH effects are controversial under various NO_x levels and seed particle conditions.

Chemical components of SOA are important, on which climate- and health-relevant properties of particles are dependent. Chemical compositions of SOA from aromatics-NO_x photooxidation have been investigated by GC/MS analysis (Forstner et al., 1997). Nevertheless, this study was only performed at 15-25% RH and high temperature at GC injection ports can easily decompose some low-volatile substances in SOA. FTIR was also used to study chemical compositions of SOA from aromatics-NO_x photooxidation under different RH conditions, in which the information of functional groups in SOA was

provided (Jia and Xu, 2014, 2018). The recent study on SOA components from toluene-OH system under both dry and humid conditions were analysed via HRMS (Hinks et al., 2018). Although the information of chemical compositions in SOA has been given, the analysis and the mechanism of RH effects still need to be further studied.

The reaction of *m*-xylene-OH system forms peroxy radicals (RO_2) that can rapidly react with HO_2 to form RO (R2a) and ROOH (R2b). RO finally forms carbonylic products, such as (methyl) glyoxal and other SOA precursors (Jenkin et al., 2003; Hallquist et al., 2009; Carlton et al., 2010; Carter and Heo, 2013). In most recent studies, RO_2 autoxidation has been observed that leads to the formation of higher-functionalized RO_2 radicals and the further formation of highly oxygenated molecules (HOMs) (Wang et al., 2017; Molteni et al., 2018). Self- or cross-reactions of RO_2 radicals were also found, leading to the formation of accretion products (R1c), especially HOM dimers, as well as RO, ROH and $R_{-H}O$ (R1a and b) (Berndt et al., 2018). However, the RH effects on the mechanism of *m*-xylene SOA formation are not well studied.

$$ROO\cdot + R'OO\cdot \rightarrow RO\cdot + R'O\cdot + O_2 \quad \text{(R1a)}$$

$$\rightarrow ROH + R'_{-H}O + O_2 \quad \text{(R1b)}$$

$$\rightarrow ROOR' + O_2 \quad \text{(R1c)}$$

$$ROO\cdot + HOO\cdot \rightarrow RO\cdot + HO\cdot + O_2 \quad \text{(R2a)}$$

$$\rightarrow ROOH + O_2 \quad \text{(R2b)}$$

RH effects on SOA formation from *m*-xylene under low NO_x condition have not been studied well. In the present study, we present the results from the experiments about the SOA formation from the OH-initiated oxidation of *m*-xylene in the absence of seed particles in a smog chamber. Both the SOA yields and chemical components under both low and high RH conditions will be reported. The underlying mechanism of SOA formation for these different conditions will be also discussed.

2 Experimental materials and methods

2.1 Equipment and reagents

Experiments of *m*-xylene photooxidation were performed in a 1 m^3 Teflon FEP film reactor (DuPont 500A, USA) in an indoor smog chamber, which is similar to our previous works (Jia and Xu, 2014, 2016, 2018; Ge et al., 2016, 2017b, c, a). So only a brief introduction is presented here. A light source was provided by 96 lamps (F40BLB, GE; UVA-340, Q-Lab, USA) inside the chamber to simulate the UV band of solar spectrum in the troposphere. The NO_2 photolysis rate was determined to be 0.23 min^{-1}, which was used to reflect the light intensity in the reactor. To remove the electric charge on the surface of the FEP reactor, two ionizing air blowers were equipped in the chamber and were used throughout each experiment.

The background gas was zero air, which was generated from Zero Air Supply and CO Reactor (Model 111 and 1150, Thermo Scientific, USA) and further purified by hydrocarbon traps (BHT-4, Agilent, USA). The desired RH in the reactor was obtained by bubbling dry zero air through ultrapure water (Milli Q, 18MU, Millipore Ltd., USA). The RH and temperature in the reactor were measured by a hygrometer (Model 645, Testo AG, Germany).

Atmos. Chem. Phys. Discuss., https://doi.org/10.5194/acp-2019-20
Manuscript under review for journal Atmos. Chem. Phys.
Discussion started: 18 February 2019

Throughout each experiment, the background NO_x concentration in the reactor was lower than 1 ppb and OH radicals were provided from H_2O_2 photolysis. Hydrogen peroxide was introduced to the reactor by evaporating a measured volume of H_2O_2 solution (30 wt %) into a zero air stream over a period of 30 min to the desired concentration of 20 ppm. Though the H_2O_2 level was not measured, it was estimated through the measured volume of H_2O_2 solution evaporated. *m*-Xylene (99%, Alfa Aesar) was introduced to the reactor subsequently using the same approach. No seed particles were introduced artificially.

2.2 Monitoring and analysis

The concentration of *m*-xylene in the reactor was measured with a gas chromatograph-mass spectrometer (GC-MS, Model 7890A GC and Model 5975C mass selective detector, Agilent, USA), which was equipped with a thermal desorber (Master TD, Dani, Italy). The size distribution and concentrations of particles were monitored with a scanning mobility particle sizer (SMPS, Model 3936, TSI, USA). The particle wall loss constant has been determined to be 3.0×10^{-5} s^{-1} at low RH and 6.0×10^{-5} s^{-1} at high RH conditions. The particles measured by SMPS consisted of liquid water content (LWC) and SOA at certain RH conditions. To determine the SOA concentration, LWC was determined at the end of each experiment except for the low RH ones, which was based on the method in a previous study (Jia and Xu, 2018).

For the analysis of functional groups of the chemical composition in SOA from *m*-xylene-OH irradiation, the SOA samples were collected and determined by FTIR (Fourier transform infrared spectrometer). The particles were collected on a ZnSe disk using a Dekati low-pressure impactor (DLPI, Dekati Ltd., Finland) at the end of each experiment (Ge et al., 2016; Jia and Xu, 2016). Then, the ZnSe disk was put in a FTIR (Nicolet iS10, Thermos Fisher, USA) for the measurement of functional groups of the chemical composition in SOA samples.

To obtain the detailed information of chemical composition, SOA particles were sampled using the Particle into Liquid Sampler (PILS, model 4001, BMI, USA). The flow rate of sample gas was around 11 L min^{-1}, and the output flow rate of liquid sample was 0.05 mL min^{-1}. Two denuders were used to remove the VOCs and acids in the sample gas. SOA liquid samples collected by PILS were finally transferred into vials for subsequent analysis. Operatively, the blank measurements were obtained by replacing the sample gas with zero air collected in vials.

The accurate mass of organic compounds in SOA and their MS/MS fragmentations were measured by the ultrahigh performance liquid chromatograph (UPLC, Ultimate 3000, Thermo Scientific, USA)-heated-electrospray ionization-high-resolution orbitrap mass spectrometer (HESI-HRMS, Q Exactive, Thermo Scientific, USA). Methanol (Optima™ LC/MS Grade, Fisher Chemical, USA) was used as the eluent in UPLC system. The elution flow rate was 0.2 mL min^{-1}, and the overall run time was 5 minutes. The injection volume was 20 μL. The acquired mass spectrum of SOA was in the range of 80-1000 Da. The HESI source was conducted in both positive and negative ion modes using the optimum method for characterization of organic compounds. We used the Thermo Scientific Xcalibur software (Thermo Fisher Scientific Inc., USA) to analyse the data from HRMS. To calculate the elemental compositions of compounds, the accurate mass measurements were used. For further analysis of the data from the second stage of data-dependent mass spectrometry

(ddMS^2), the Mass Frontier program (Version 7.0, Thermo Fisher Scientific Inc., USA) was used in order to simulate breaking the ions into fragments for comparison with the measured fragments to assist in identifying the structures. The reaction pathways and products of *m*-xylene-OH photooxidation in Master Chemical Mechanism (MCM v3.3.1, the website at http://mcm.leeds.ac.uk/MCM; last accessed October 16, 2017) was used for analysis of the products measured by HRMS (Jenkin et al., 2003; Jia and Xu, 2014).

3. Results and discussion

3.1 RH effects on SOA yields

Figure 1 shows the wall-loss-corrected particle mass concentration as a function of photooxidation reaction time for *m*-xylene-OH systems under both the low-RH and the high-RH conditions. It can be clearly seen that there is a large difference in the maximum mass concentration between low and high RHs. The maximum mass concentrations fitted are 130.1 and 94.3 μg m^{-3} at low RHs, whereas they are 1.9 and 0.8 μg m^{-3} at high RHs, with the largest difference being over ten times. The RH effect was reproducible when the initial *m*-xylene concentration was changed under similar conditions. To obtain the particle mass concentrations and SOA yield, an SOA density of 1.4 g cm^{-3} was used (Ng et al., 2007; Sato et al., 2007). It should be noted that the fairly large scatter in the mass concentrations of SOA in Fig. 1 was observed, which mainly results from the uncertainty of SOA measurement by SMPS instrument. The interval of SOA data sampled by SMPS was 5 minutes, for which the sampling frequency was relatively low. SMPS measurement uncertainty is mainly dominated by size-dependent aerosol charging efficiency uncertainties and CPC sampling flow rate variability. The size-dependent aerosol charging efficiency is typically characterized by an accuracy of ± 10% (Jiang et al., 2014). The combination of various uncertainties, including SMPS measurement, sampling and even conversion of mass concentration from number concentration leads to the fairly large scatter in Fig. 1.

We used the definition of the ratio of the SOA mass to the consumed *m*-xylene mass to calculate the SOA yield at the end of each experiment. Under high RH condition, LWC accounts for a large proportion of particles (Jia and Xu, 2018). So, when SOA yield is calculated at high RH, the LWC has to be subtracted. It should be pointed out that SOA concentrations for high RH conditions were slightly underestimated due to the LWC measurement, as the dissolved species that are probably volatile/semi-volatile compounds, would evaporate back into the gas phase when the aerosol water is removed.

Experimental conditions and SOA concentrations at the end of the experiments in *m*-xylene-OH oxidation system are summarized in Table 1. The SOA yields at low RH are 12.7-13.8%, while those at high RH are only around 0.8-1.9%. Both mass concentrations and SOA yields at low RH are an order of magnitude larger than those at high RH. It should be noticed that temperatures at high RH are slightly higher than those at low RH. Though low temperature can lead to a high SOA yield, the difference of temperature between low and high RH conditions in this study is lower than two degree, which cannot lead to a significantly different SOA yields to affect the result (Qi et al., 2010).

In the most recent study on toluene SOA formation conducted without seed particles (Hinks et al., 2018), the SOA yield at low NO_x level was 15% under dry conditions (< 2% RH) and 1.9% under humid conditions (89% RH), with the ratio of two yields between dry and humid conditions being over 7.5. The toluene SOA produced under high RH conditions were significantly suppressed, in which the tendency of RH effects on SOA yield was very similar with our study, though the difference of SOA yield between low and high RH conditions in Hinks et al (2018) was slightly smaller than that in this study. The small difference of RH effects between Hinks et al. and our study is likely associated with the difference in experimental conditions, including RHs and initial VOCs and H_2O_2 concentrations, in addition to different species. This comparison demonstrates that different species of toluene and *m*-xylene of aromatics pose very similar RH effects under low-NOx conditions. Hinks et al. attributed the suppression of SOA yields by elevated RH to the lower level of oligomers generated by condensation reactions and the reduced mass loading at high RH. In a study on an SOA model for toluene oxidation, it could be found that the SOA yield at low NO_x level was 28-30% under low RH conditions (17-18% RH) and 20-25% under moderate RH conditions (48% RH) (Cao and Jang, 2010), but they did not focus on the RH effect to give an explanation. As the difference of RH was only ~30%, the RH effect on SOA yields was not as significant as those in Hinks et al and this study. Ng et al. have investigated the yields of SOA formed from *m*-xylene-OH system at low RH (4-6%) under low NO_x conditions (Ng et al., 2007). They obtained that the SOA yields were in the range of 35.2-40.4% in the presence of seed particles. The SOA yields were larger than that of this study, as they conducted the experiments under different irradiation time and with inorganic seed particles. These seed particles can provide not only surface for chemical reactions, but also acidic and aqueous environments that can promote the SOA formation (Jang et al., 2002; Liu et al., 2018; Faust et al., 2017). In a study on chemical oxidative potential of SOA (Tuet et al., 2017), it was observed that the concentration of SOA from *m*-xylene irradiation at low NO_x level under dry condition was much larger than that under humid condition (89.3 μg m^{-3} at < 5% RH and 13.9 μg m^{-3} at 45% RH), but they did not calculate the *m*-xylene SOA yields or give an explanation for the RH effect. However, a previous study under high NO_x conditions (Zhou et al., 2011) found that the effect of RH on SOA yields from aromatics photooxidation were positive, which obtained opposite results to our study. LWC was used to account for this positive effect as it could promote SOA formation through aqueous chemistry (Jia and Xu, 2014; Wang et al., 2016; Faust et al., 2017; Liu et al., 2018).

3.2 RH effects on functional groups of SOA

Figure 2 shows the FTIR spectra of particles from the photooxidation of *m*-xylene-OH experiments under both low (Exp. 2) and high (Exp. 3) RH conditions. As shown in Fig. 2, the SOA from *m*-xylene-OH experiments can be obviously observed under both two RH conditions. The intensities of all functional groups from the low RH experiment are much higher than those from the high RH experiment, which is consistent with the reduced SOA yields under elevated RH conditions.

The assignment and the intensity of the FTIR absorption frequencies is summarized in Table 2. The broad absorption at 3600-2400 cm^{-1} is O-H stretching vibration in phenol, hydroxyl and carboxyl groups. The sharp absorption at 1720 cm^{-1} is the C=O stretching vibration in carboxylic acids, formate esters, aldehydes and ketones. The absorptions at 1605 cm^{-1} match

the ionized carboxylic groups and bending vibration of liquid water. The absorptions at 1415 cm^{-1} match the deformation of CO-H, phenolic O-H and C-O. The absorptions at 1180 cm^{-1} match the C-O-C stretching of polymers, C-O and OH of COOH groups; C-O and OH of COOH groups. The absorptions at 1080 cm^{-1} match the C-C-OH stretching of alcohols.

The absorption intensity at ~3200 cm^{-1} that is identified as the hydroxyl group is used to be a representative for reflection of the SOA formation. As well, Table 2 gives the ratio of intensities at high RH to those at low RH to compare the difference of relative intensities of functional groups. The intensities of functional groups are obviously suppressed at high RH, but the extents of the suppression for different functional groups are basically divided into two types. The ratios of O-H, C=O and C-C-OH groups are similar, with the value being below 0.35, whereas the ratios of COO-, CO-H, C-O-C, C-O and OH in COOH are above 0.48. In the previous study, the band at 1080 cm^{-1} is considered to be mainly from glyoxal hydrate (Jia and Xu, 2014) as glyoxal is highly water soluble and can be readily absorbed to the aerosol phase at above 26% RH (Hastings et al., 2005; Ip et al., 2009; Waxman et al., 2015). The ratio of C-C-OH is slightly higher than that of O-H, which indicates the glyoxal is hydrolyzed into hydroxyl at high RH whereas the process is not significant in this study. The ratio of the C-O-C group is significantly higher than the C=O group, which can be explained by oligomerization with the formation of C-O-C at high RH. Nevertheless, the FTIR results cannot provide further information to well explain the differences of SOA yields between low and high RH.

3.3 RH effects on mass spectra of SOA

We selected the sample mass spectra whose intensities are larger than 10^5 under the low RH condition and corresponding mass spectra under the high RH condition, followed by the blank mass spectra deduction. The blank-deducting mass spectra of SOA formed from *m*-xylene-OH photooxidation under low and high RH conditions in both positive and negative ion modes are presented in Fig. 3, which is plotted as a function of the mass-to-charge ratio. It should be noted that the Y-axis scales for low and high RH are largely different, 10^6 at low RH and 10^5 at high RH. As shown in Fig. 3, a visible decrease in the overall peak intensities for both positive and negative ion modes can be obviously observed as the RH elevates, which is consistent with the result that the SOA mass concentration is lower at high RH. In addition, it is obvious that the number of peaks is less under the high RH condition.

As shown in Fig. 3, where the m/z values of SOA samples are close for both low and high conditions, the absolute and relative intensities of the peaks are much different, indicating that RH significantly affects the concentration of SOA components. It should be pointed out that the signal intensities may be biased by the ionizing properties and do not necessarily represent the actual distribution of the neutral compounds.

Table 3 lists the peaks whose intensities are larger than 10^6 of low RH samples and the structure can be proposed according to the gas-phase chemical mechanism of *m*-xylene-OH photooxidation included in MCM and the fragments from MS/MS analysed with Mass Frontier. In the positive ion mode, an $[M+H]^+$ ion of m/z = 137.05962 at low RH and 137.05931 at high RH is assigned as a molecular ion formula of $C_8H_9O_2^+$ that has a mass difference of Δ = 0.6 and 1.0 mDa for low and high RH, respectively. The structure of identified compound $C_8H_8O_2$ is proposed to be 2,6-dimethyl-1,4-benzoquinone, the

fragments of which from MS/MS match those from simulation of the Mass Frontier program. This compound was also identified and quantified in a previous study on SOA compositions from *m*-xylene-NO_x irradiation using the method of GC-MS analysis with authentic standards (Forstner et al., 1997). Thus, 2,6-dimethyl-1,4-benzoquinone was the SOA component partitioning into particle phase from the gas phase. The measured ion of m/z = 155.07013 at low RH and 155.06985 at high RH is assigned as a molecular ion formula of $C_8H_{11}O_3^+$ that has Δ = 1.2 and 1.5 mDa, and its structure is proposed to be O=CC1(C)OC1C=CC(=O)C, an oxidized unsaturated epoxide. The measured ion of m/z = 171.06509 at low RH and 171.06488 at high RH is assigned as a molecular ion formula of $C_8H_{11}O_5^+$ that has Δ = 1.2 and 1.4 mDa, the structure of which is proposed to be a bicyclic peroxide. The measured ion of m/z = 187.06003 at low RH and 187.05678 at high RH is assigned as a molecular ion formula of $C_8H_{11}O_5^+$ that has Δ = 1.2 and 4.4 mDa, whose structure is proposed to be O=CC1(C)OC1C(O)C(=O)C(=O)C. All these SOA components are suppressed to almost disappear at high RH, except for 2,6-dimethyl-1,4-benzoquinone.

For rough quantification of the RH effect, the peaks in Figure 3 were assigned with the number of carbon atoms. The intensities of the peaks with the same number of carbon atoms (nC) are summed, which are presented in Figure 4. It should be noted that the Y-axis scales at low and high RHs are largely different, with a label step of 4.0×10^6 at low RH and 4.0×10^5 at high RH in the positive ion mode, 5.0×10^6 at low RH and 1.0×10^5 at high RH in the negative ion mode. The compounds with nC > 8, larger number of carbon atoms than *m*-xylene, are proposed to be oligomers that account for a large mass fraction of SOA due to their large molecular weights and lower volatilities, though their peak intensities are lower. As a result, the processes for formation of such compounds play an important role in the formation of SOA. It can be obviously observed that the peak intensities are much lower at high RH in the negative ion mode than that in the positive mode, indicating that the decrease of the compounds obtained in the negative ion mode account for a larger decrease at high RH. Moreover, in the positive ion mode, compounds with nC > 8, especially those with nC > 10, account for more SOA mass at high RH than at low RH, which can be observed by the increase of relative intensities of oligomers. However, in the negative ion mode, compounds with nC > 8 account for less SOA mass at high RH. In the positive ion mode, 15 compounds with nC = 10 identified with HRMS dominate the spectrum. To get more information, the MS/MS data analysis was further carried out. We found that the fragment with m/z = 61.03 obtained by the MS/MS was observed in nine out of the fifteen compounds, which is assigned as a molecular ion formula of $C_2H_5O_2^+$. The sum of peak intensities of these nine compounds accounts for about 70% of the sum of peak intensities of these fifteen nC = 10 compounds. The structure of this fragment is possibly proposed to be glycolaldehyde ($C_2H_4O_2$), which has been observed previously in the oxidation of *m*-xylene (Cocker et al., 2001). It has been implied that the oligomerization of glycolaldehyde took place in the study of formation of toluene SOA (Hinks et al., 2018). This demonstrates that the nC = 10 compounds are mainly from the oligomerization of glycolaldehyde and nC = 8 monomers.

Atmos. Chem. Phys. Discuss., https://doi.org/10.5194/acp-2019-20
Manuscript under review for journal Atmos. Chem. Phys.
Discussion started: 18 February 2019

Atmospheric Chemistry and Physics Discussions

3.4 Proposed mechanism of RH effects on SOA formation

It has been confirmed that glyoxal is an important SOA precursor via oligomerization (Jang et al., 2002; Kamens et al., 2011; Zhou et al., 2011). An explanation for the large difference of SOA yields and composition between low and high RH is proposed that water is directly involved in the chemical mechanism and further affects the SOA growth. However, in some particle-phase accretion equilibrium reactions, water is involved as a by-product. The elevated RH alters the equilibrium of reaction toward the decrease of products (Nguyen et al., 2011; Hinks et al., 2018). The hydrolysis of oligomers would be facilitated by the elevated RH after the oligomers are generated in gas phase and partition into particles with certain LWC. In this study and the previous study on toluene SOA formation, C_2H_2O was one of the most frequently mass difference at both RH, but the peak intensities of its relative compounds were much lower under elevated RH conditions (Hinks et al., 2018). C_2H_2O was proposed to be from the oligomerization reaction of glycolaldehyde ($C_2H_4O_2$), which can react with carbonyl compounds by aldol condensation reactions with water as the by-product. However, this mechanism cannot well explain the large different SOA yields at low and high RH.

Another possible explanation for RH effects on SOA chemical components is that RH influences the HOMs formation from *m*-xylene-OH system (Fig. 5). Reactions between *m*-xylene (C_8H_{10}) and OH radicals have two pathways, the H-abstraction from the methyl group and OH-addition to the aromatic ring, which generates products such as methylbenzaldehyde (C_8H_8O) and methylbenzyl alcohol ($C_8H_{10}O$), as shown in Scheme 1. OH-addition is the dominant pathway, as the branching ratio of H-abstraction only accounts for 4% based on the MCM simulation. OH-addition to the aromatic ring is followed by O_2-adduct and isomerization to form a carbon-centered radical, which can form a dimethylphenol ($C_8H_{10}O$) or is adducted by an O_2 molecule forming a bicyclic peroxy radical (BPR, $C_8H_{11}O_5$) (Calvert et al., 2002; Birdsall et al., 2010; Wu et al., 2014), which is called the RO_2 autoxidation. The BPR reacts with other RO_2 radicals or HO_2 forming the bicyclic oxy radical ($C_8H_{11}O_4$). This RO radical can get further reaction and finally form carbonylic products (R1a and R2a), such as (methyl) glyoxal and other SOA precursors (Jenkin et al., 2003; Hallquist et al., 2009; Carlton et al., 2010; Carter and Heo, 2013), or react with HO_2 radicals forming bicyclic hydroxyhydroperoxides (ROOH, $C_8H_{12}O_5$) (R2b), or react with other RO_2 radicals forming ROH ($C_8H_{12}O_4$) and $R_{-H}O$ ($C_8H_{10}O_4$) (R1b). The self- and cross-reactions of RO_2 radicals also form ROOR ($C_{16}H_{22}O_{10}$) or ROOR' that is the accretion products (Berndt et al., 2018; Molteni et al., 2018). The further autoxidation of BPR can form a highly-functionalized RO_2 radicals and further get reacted and finally form HOMs (Types 1 and 2 in Scheme 1) (Wang et al., 2017; Crounse et al., 2013; Ehn et al., 2014; Jokinen et al., 2015; Berndt et al., 2016). Dimethylphenol ($C_8H_{10}O$) as well as other products from termination reaction with benzene ring or double bond can react with OH radicals and get further reacted to form HOMs as well. The compounds with the number below their formulae in scheme 1 were determined by HRMS to be present in the particle phase.

The distribution of relative intensity of SOA products with same carbon number was shown in Fig. 5 to investigate the potential RH effect on HOMs. Oxidation compounds with the same carbon number but different oxygen number were observed. In the mass-to-charge (m/z) range 135-240 Da in both positive and negative ion modes, the oxidation products

contain the carbon skeleton of *m*-xylenes (monomer region, nC = 8), while in the m/z range 320-410 Da the number of carbon atoms is doubled (dimer region, nC = 16). The compounds with high O/C ratios are observed, which are generally called HOMs. In a previous study on *m*-xylene oxidation, HOM monomers including $C_8H_{10}O_{5\text{-}8}$, $C_8H_{12}O_{5\text{-}8}$ and $C_8H_{14}O_{6\text{-}8}$, and HOM dimers including $C_{16}H_{22}O_{9\text{-}12}$ and $C_{16}H_{24}O_{11}$ were obtained using CI-APi-TOF-MS (chemical ionization atmospheric pressure interface time of flight mass spectrometer) (Molteni et al., 2018), which are also determined in our study. More HOMs can be obtained in the negative ion mode where oxygen atom numbers can reach up to 8 for monomers and 12 for dimers, when compared with those in the positive ion mode. In addition, here the O/C ratio was calculated based on the O and C atom numbers in structures and peak intensities, which is 0.57 and 0.71 in the positive and negative ion modes, respectively. This also demonstrates that the compounds in the negative ion mode are much more oxygenated than those in the positive ion mode. As shown in Fig. 4, the peak intensities at high RH are much lower in the negative ion mode than in the positive mode, indicating that the decrease of the more oxygenated compounds account for the larger fraction at high RH. These high O/C ratios cannot be explained by any of the formerly known oxidization pathways except that RO_2 autoxidation is taken into consideration (Crounse et al., 2013; Barsanti et al., 2017). Both HOM monomers and dimers obviously decrease with increasing RH. RH significantly affect the formation of the HOMs. The relative intensities of compounds with same nC but larger oxygen number decrease more significantly. High RH significantly suppresses the more oxidized compounds whose volatility is lower and molecular weights are larger. Therefore, it is considered that RH suppresses the RO_2 autoxidation and further affects the SOA yield.

4. Conclusion and atmospheric implication

The current study investigates the effect of RH on SOA formation from the OH-initiated oxidation of *m*-xylene in the absence of seed particles. The elevated RH can significantly obstruct the SOA formation from the *m*-xylene-OH system, so that the SOA yield decrease from 13.8% at low RH to 0.8% at high RH, with a significant discrepancy of higher than one order of magnitude. The FTIR results of functional groups show the relative increase of the C-O-C group at high RH as compared with low RH, indicating that the oligomers from carbonyl compounds cannot well explain the suppression of SOA yield. HOMs were observed to be suppressed in the HRMS spectra. The chemical mechanism for explaining the obvious difference of RH effects on SOA formation from *m*-xylene-OH system has been proposed based on the analysis of both FTIR and HRMS measurements as well as MCM simulations. The reduced SOA at high RH is mainly ascribed to the less formation of oligomers and the suppression of RO_2 autoxidation. Together with the previous study on toluene SOA, it is conceivable that the effect of RH on the SOA yield is a common feature of SOA formation from oxidation of all OH-initiated aromatics. Although the clear pathway of the influence of H_2O on the formation of HOMs still cannot be given, which needs to be further studied in the future, our results obviously indicate that the production of SOA from aromatics in low-NO_x environments can be strongly modulated by the ambient RH. Our study highlights the role of water in the SOA

formation, which is particularly related to chemical mechanisms used to explain observed air quality and to predict chemistry in air quality models and climate models.

Author contribution

Qun Zhang and YongFu Xu designed the research. Qun Zhang carried out the experiments and analyzed the data. Long Jia provided valuable advices on the experiment operations. YongFu Xu and Long Jia provided advices on the analysis of results. Qun Zhang prepared the manuscript with contributions from all co-authors.

Acknowledgments

This work was supported by the National Key R&D Program of China (2017YFC0210005) and National Natural Science Foundation of China (No. 41375129).

References

Barsanti, K. C., Kroll, J. H., and Thornton, J. A.: Formation of low-volatility organic compounds in the atmosphere: Recent advancements and insights, J. Phys. Chem. Lett., 8, 1503-1511, 10.1021/acs.jpclett.6b02969, 2017.

Berndt, T., Richters, S., Jokinen, T., Hyttinen, N., Kurten, T., Otkjaer, R. V., Kjaergaard, H. G., Stratmann, F., Herrmann, H., Sipila, M., Kulmala, M., and Ehn, M.: Hydroxyl radical-induced formation of highly oxidized organic compounds, Nat. Commun., 7, 13677, 10.1038/ncomms13677, 2016.

Berndt, T., Scholz, W., Mentler, B., Fischer, L., Herrmann, H., Kulmala, M., and Hansel, A.: Accretion product formation from self- and cross-reactions of RO_2 radicals in the atmosphere, Angew. Chem. Int. Ed., 57, 3820-3824, 10.1002/anie.201710989, 2018.

Birdsall, A. W., Andreoni, J. F., and Elrod, M. J.: Investigation of the role of bicyclic peroxy radicals in the oxidation mechanism of toluene, J. Phys. Chem. A, 114, 10655-10663, 10.1021/jp105467e, 2010.

Bloss, C., Wagner, V., Jenkin, M. E., Volkamer, R., Bloss, W. J., Lee, J. D., Heard, D. E., Wirtz, K., Martin-Reviejo, M., Rea, G., Wenger, J. C., and Pilling, M. J.: Development of a detailed chemical mechanism (MCMv3.1) for the atmospheric oxidation of aromatic hydrocarbons, Atmos. Chem. Phys., 5, 641-664, 10.5194/acp-5-641-2005, 2005.

Calvert, J. G., Atkinson, R., Becker, K. H., Kamens, R. M., Seinfeld, J. H., Wallington, T. H., and Yarwood, G.: The mechanisms of atmospheric oxidation of the aromatic hydrocarbons, Oxford University Press, 2002.

Cao, G., and Jang, M.: An SOA model for toluene oxidation in the presence of inorganic aerosols, Environ. Sci. Technol., 44, 727-733, 10.1021/es901682r, 2010.

Carlton, A. G., Bhave, P. V., Napelenok, S. L., Edney, E. O., Golam, S., Pinder, R. W., Pouliot, G. A., and Marc, H.: Model representation of secondary organic aerosol in CMAQv4.7, Environ. Sci. Technol., 44, 8553-8560, 10.1021/es100636q, 2010.

Carter, W. P. L., and Heo, G.: Development of revised SAPRC aromatics mechanisms, Atmos. Environ., 77, 404-414, 10.1016/j.atmosenv.2013.05.021, 2013.

Cocker, D. R., Mader, B. T., Kalberer, M., Flagan, R. C., and Seinfeld, J. H.: The effect of water on gas-particle partitioning of secondary organic aerosol: II. *m*-xylene and 1,3,5-trimethylbenzene photooxidation systems, Atmos. Environ., 35, 6073-6085, 10.1016/s1352-2310(01)00405-8, 2001.

Crounse, J. D., Nielsen, L. B., Jørgensen, S., Kjaergaard, H. G., and Wennberg, P. O.: Autoxidation of organic compounds in the atmosphere, J. Phys. Chem. Lett., 4, 3513-3520, 10.1021/jz4019207, 2013.

Ding, X., Wang, X.-M., Gao, B., Fu, X.-X., He, Q.-F., Zhao, X.-Y., Yu, J.-Z., and Zheng, M.: Tracer-based estimation of secondary organic carbon in the Pearl River Delta, south China, J. Geophys. Res., 117, D05313, 10.1029/2011jd016596, 2012.

Ehn, M., Thornton, J. A., Kleist, E., Sipilä, M., Junninen, H., Pullinen, I., Springer, M., Rubach, F., Tillmann, R., and Lee, B.: A large source of low-volatility secondary organic aerosol, Nature, 506, 476-479, 10.1038/nature13032, 2014.

Faust, J. A., Wong, J. P., Lee, A. K., and Abbatt, J. P.: Role of Aerosol Liquid Water in Secondary Organic Aerosol Formation from Volatile Organic Compounds, Environ. Sci. Technol., 51, 1405-1413, 10.1021/acs.est.6b04700, 2017.

Finlayson-Pitts, B. J., and Pitts Jr., J. N.: Chapter 6-Rates and mechanisms of gas-phase reactions in irradiated organic-NO_x-air mixtures, in: Chemistry of the Upper and Lower Atmosphere, Academic Press, San Diego, 179-263, 2000.

Forstner, H. J. L., Flagan, R. C., and Seinfeld, J. H.: Secondary organic aerosol from the photooxidation of aromatic hydrocarbons: Molecular composition, Environ. Sci. Technol., 31, 1345-1358, 10.1021/es9605376, 1997.

Ge, S., Xu, Y., and Jia, L.: Secondary organic aerosol formation from ethyne in the presence of NaCl in a smog chamber, Environ. Chem., 13, 699-710, 10.1071/en15155, 2016.

Ge, S., Xu, Y., and Jia, L.: Secondary organic aerosol formation from ethylene ozonolysis in the presence of sodium chloride, J. Aerosol Sci., 106, 120-131, 10.1016/j.jaerosci.2017.01.009, 2017a.

Ge, S., Xu, Y., and Jia, L.: Effects of inorganic seeds on secondary organic aerosol formation from photochemical oxidation of acetone in a chamber, Atmos. Environ., 170, 205-215, 10.1016/j.atmosenv.2017.09.036, 2017b.

Ge, S., Xu, Y., and Jia, L.: Secondary organic aerosol formation from propylene irradiations in a chamber study, Atmos. Environ., 157, 146-155, 10.1016/j.atmosenv.2017.03.019, 2017c.

Hallquist, M., Wenger, J. C., Baltensperger, U., Rudich, Y., Simpson, D., Claeys, M., Dommen, J., Donahue, N. M., George, C., Goldstein, A. H., Hamilton, J. F., Herrmann, H., Hoffmann, T., Iinuma, Y., Jang, M., Jenkin, M. E., Jimenez, J. L., Kiendler-Scharr, A., Maenhaut, W., McFiggans, G., Mentel, T. F., Monod, A., Prévôt, A. S. H., Seinfeld, J. H., Surratt, J. D., Szmigielski, R., and Wildt, J.: The formation, properties and impact of secondary organic aerosol: current and emerging issues, Atmos. Chem. Phys., 9, 5155-5236, 10.5194/acp-9-5155-2009, 2009.

Hansen, J. E., and Sato, M.: Trends of measured climate forcing agents, Proc. Natl. Acad. Sci. U. S. A., 98, 14778-14783, 10.1073/pnas.261553698, 2001.

Hastings, W. P., Koehler, C. A., Bailey, E. L., and De Haan, D. O.: Secondary organic aerosol formation by glyoxal hydration and oligomer formation: humidity effects and equilibrium shifts during analysis, Environ. Sci. Technol., 39, 8728-8735, 10.1021/es050446l, 2005.

Healy, R. M., Temime, B., Kuprovskyte, K., and Wenger, J. C.: Effect of relative humidity on gas/particle partitioning and aerosol mass yield in the photooxidation of *p*-xylene, Environ. Sci. Technol., 43, 1884-1889, 10.1021/es802404z, 2009.

Hinks, M. L., Montoya-Aguilera, J., Ellison, L., Lin, P., Laskin, A., Laskin, J., Shiraiwa, M., Dabdub, D., and Nizkorodov, S. A.: Effect of relative humidity on the composition of secondary organic aerosol from the oxidation of toluene, Atmos. Chem. Phys., 18, 1643-1652, 10.5194/acp-18-1643-2018, 2018.

Huang, R. J., Zhang, Y., Bozzetti, C., Ho, K. F., Cao, J. J., Han, Y., Daellenbach, K. R., Slowik, J. G., Platt, S. M., Canonaco, F., Zotter, P., Wolf, R., Pieber, S. M., Bruns, E. A., Crippa, M., Ciarelli, G., Piazzalunga, A., Schwikowski, M., Abbaszade, G., Schnelle-Kreis, J., Zimmermann, R., An, Z., Szidat, S., Baltensperger, U., El Haddad, I., and Prevot, A. S.: High secondary aerosol contribution to particulate pollution during haze events in China, Nature, 514, 218-222, 10.1038/nature13774, 2014.

Ip, H. S. S., Huang, X. H. H., and Yu, J. Z.: Effective Henry's law constants of glyoxal, glyoxylic acid, and glycolic acid, Geophys. Res. Lett., 36, L01802, 10.1029/2008gl036212, 2009.

Jacobson, M. C., Hansson, H. C., Noone, K. J., and Charlson, R. J.: Organic atmospheric aerosols: Review and state of the science, Rev. Geophys., 38, 267-294, 10.1029/1998rg000045, 2000.

Jang, M., Czoschke, N. M., Lee, S., and Kamens, R. M.: Heterogeneous atmospheric aerosol production by acid-catalyzed particle-phase reactions, Science, 298, 814-817, 10.1126/science.1075798, 2002.

Jenkin, M. E., Saunders, S. M., Wagner, V., and Pilling, M. J.: Protocol for the development of the Master Chemical Mechanism, MCM v3 (Part B): tropospheric degradation of aromatic volatile organic compounds, Atmos. Chem. Phys., 3, 181-193, 10.5194/acp-3-181-2003, 2003.

Jia, L., and Xu, Y.: Effects of relative humidity on ozone and secondary organic aerosol formation from the photooxidation of benzene and ethylbenzene, Aerosol Sci. Technol., 48, 1-12, 10.1080/02786826.2013.847269, 2014.

Jia, L., and Xu, Y.: Ozone and secondary organic aerosol formation from Ethylene-NOx -NaCl irradiations under different relative humidity conditions, J. Atmos. Chem., 73, 81-100, 10.1007/s10874-015-9317-1, 2016.

Jia, L., and Xu, Y.: Different roles of water in secondary organic aerosol formation from toluene and isoprene, Atmos. Chem. Phys., 18, 8137-8154, 10.5194/acp-18-8137-2018, 2018.

Jiang, J., Kim, C., Wang, X., Stolzenburg, M. R., Kaufman, S. L., Qi, C., Sem, G. J., Sakurai, H., Hama, N., and McMurry, P. H.: Aerosol charge fractions downstream of six bipolar chargers: Effects of ion source, source activity, and flowrate, Aerosol Sci. Technol., 48, 1207-1216, 10.1080/02786826.2014.976333, 2014.

Jokinen, T., Sipilä, M., Richters, S., Kerminen, V. M., Paasonen, P., Stratmann, F., Worsnop, D., Kulmala, M., Ehn, M., and Herrmann, H.: Rapid autoxidation forms highly oxidized RO_2 radicals in the atmosphere, Angew. Chem. Int. Ed., 53, 14596-14600, 10.1002/anie.201408566, 2015.

Kamens, R. M., Zhang, H., Chen, E. H., Zhou, Y., Parikh, H. M., Wilson, R. L., Galloway, K. E., and Rosen, E. P.: Secondary organic aerosol formation from toluene in an atmospheric hydrocarbon mixture: Water and particle seed effects, Atmos. Environ., 45, 2324-2334, 10.1016/j.atmosenv.2010.11.007, 2011.

Kanakidou, M., Seinfeld, J. H., Pandis, S. N., Barnes, I., Dentener, F. J., Facchini, M. C., Dingenen, R. V., Ervens, B., Nenes, A., Nielsen, C. J., Swietlicki, E., Putaud, J. P., Balkanski, Y., Fuzzi, S., Horth, J., Moortgat, G. K., Winterhalter, R., Myhre, C. E. L., Tsigaridis, K., Vignati, E., Stephanou, E. G., and Wilson, J.: Organic aerosol and global climate modelling: a review, Atmos. Chem. Phys., 5, 1053-1123, 10.5194/acp-5-1053-2005, 2005.

Khoder, M. I.: Ambient levels of volatile organic compounds in the atmosphere of Greater Cairo, Atmos. Environ., 41, 554-566, 10.1016/j.atmosenv.2006.08.051, 2007.

Liu, T., Huang, D., Li, Z., Liu, Q., Chan, M., and Chan, C. K.: Comparison of secondary organic aerosol formation from toluene on initially wet and dry ammonium sulfate particles at moderate relative humidity, Atmos. Chem. Phys., 18, 5677-5689, 10.5194/acp-18-5677-2018, 2018.

Molteni, U., Bianchi, F., Klein, F., El Haddad, I., Frege, C., Rossi, M. J., Dommen, J., and Baltensperger, U.: Formation of highly oxygenated organic molecules from aromatic compounds, Atmos. Chem. Phys., 18, 1909-1921, 10.5194/acp-18-1909-2018, 2018.

Ng, N. L., Kroll, J. H., Chan, A. W. H., Chhabra, P. S., Flagan, R. C., and Seinfeld, J. H.: Secondary organic aerosol formation from *m*-xylene, toluene, and benzene, Atmos. Chem. Phys., 7, 3909-3922, 10.5194/acp-7-3909-2007, 2007.

Nguyen, T. B., Roach, P. J., Laskin, J., Laskin, A., and Nizkorodov, S. A.: Effect of humidity on the composition of isoprene photooxidation secondary organic aerosol, Atmos. Chem. Phys., 11, 6931-6944, 10.5194/acp-11-6931-2011, 2011.

Odum, J. R., Jungkamp, T. P., Griffin, R. J., Flagan, R. C., and Seinfeld, J. H.: The atmospheric aerosol-forming potential of whole gasoline vapor, Science, 276, 96-99, 10.1126/science.276.5309.96, 1997.

Offenberg, J. H., Lewis, C. W., Lewandowski, M., Jaoui, M., Kleindienst, T. E., and Edney, E. O.: Contributions of toluene and α-pinene to SOA formed in an irradiated toluene/α-pinene/NO_x/air mixture: comparison of results using ^{14}C content and SOA organic tracer methods, Environ. Sci. Technol., 41, 3972-3976, 10.1021/es070089+, 2007.

Qi, L., Nakao, S., Tang, P., and Cocker, D. R., III: Temperature effect on physical and chemical properties of secondary organic aerosol from *m*-xylene photooxidation, Atmos. Chem. Phys., 10, 3847-3854, 10.5194/acp-10-3847-2010, 2010.

Sato, K., Hatakeyama, S., and Imamura, T.: Secondary organic aerosol formation during the photooxidation of toluene: NO_x dependence of chemical composition, J. Phys. Chem. A, 111, 9796-9808, 10.1021/jp071419f, 2007.

Seinfeld, J. H., and Pandis, S. N.: Atmospheric chemistry and physics: From air pollution to climate change, 3rd ed., Wiley, Hoboken, 2016.

Spracklen, D. V., Jimenez, J. L., Carslaw, K. S., Worsnop, D. R., Evans, M. J., Mann, G. W., Zhang, Q., Canagaratna, M. R., Allan, J., Coe, H., McFiggans, G., Rap, A., and Forster, P.: Aerosol mass spectrometer constraint on the global secondary organic aerosol budget, Atmos. Chem. Phys., 11, 12109-12136, 10.5194/acp-11-12109-2011, 2011.

Tuet, W. Y., Chen, Y., Xu, L., Fok, S., Gao, D., Weber, R. J., and Ng, N. L.: Chemical oxidative potential of secondary organic aerosol (SOA) generated from the photooxidation of biogenic and anthropogenic volatile organic compounds, Atmos. Chem. Phys., 17, 839-853, 10.5194/acp-17-839-2017, 2017.

Wang, S., Wu, R., Berndt, T., Ehn, M., and Wang, L.: Formation of Highly Oxidized Radicals and Multifunctional Products from the Atmospheric Oxidation of Alkylbenzenes, Environ. Sci. Technol., 51, 8442-8449, 10.1021/acs.est.7b02374, 2017.

Wang, Y., Luo, H., Jia, L., and Ge, S.: Effect of particle water on ozone and secondary organic aerosol formation from benzene-NO_2-NaCl irradiations, Atmos. Environ., 140, 386-394, 10.1016/j.atmosenv.2016.06.022, 2016.

Warren, B., Song, C., and Cocker, D. R., III: Light intensity and light source influence on secondary organic aerosol formation for the *m*-xylene/NO_x photooxidation system, Environ. Sci. Technol., 42, 5461-5466, 10.1021/es702985n, 2008.

Waxman, E. M., Elm, J., Kurten, T., Mikkelsen, K. V., Ziemann, P. J., and Vokamer, R.: Glyoxal and Methylglyoxal Setschenow Salting Constants in Sulfate, Nitrate, and Chloride Solutions: Measurements and Gibbs Energies, Environ. Sci. Technol., 49, 11500-11508, 10.1021/acs.est.5b02782, 2015.

Wu, R., Pan, S., Li, Y., and Wang, L.: Atmospheric oxidation mechanism of toluene, J. Phys. Chem. A, 118, 4533-4547, 10.1021/jp500077f, 2014.

Zhang, X., Cappa, C. D., Jathar, S. H., McVay, R. C., Ensberg, J. J., Kleeman, M. J., and Seinfeld, J. H.: Influence of vapor wall loss in laboratory chambers on yields of secondary organic aerosol, Proc. Natl. Acad. Sci. U. S. A., 111, 5802-5807, 10.1073/pnas.1404727111, 2014.

Zhao, Y., Saleh, R., Saliba, G., Presto, A. A., Gordon, T. D., Drozd, G. T., Goldstein, A. H., Donahue, N. M., and Robinson, A. L.: Reducing secondary organic aerosol formation from gasoline vehicle exhaust, Proc. Natl. Acad. Sci. U. S. A., 114, 6984-6989, 10.1073/pnas.1620911114, 2017.

Zhou, Y., Zhang, H., Parikh, H. M., Chen, E. H., Rattanavaraha, W., Rosen, E. P., Wang, W., and Kamens, R. M.: Secondary organic aerosol formation from xylenes and mixtures of toluene and xylenes in an atmospheric urban hydrocarbon mixture: Water and particle seed effects (II), Atmos. Environ., 45, 3882-3890, 10.1016/j.atmosenv.2010.12.048, 2011.

Atmos. Chem. Phys. Discuss., https://doi.org/10.5194/acp-2019-20
Manuscript under review for journal Atmos. Chem. Phys.
Discussion started: 18 February 2019

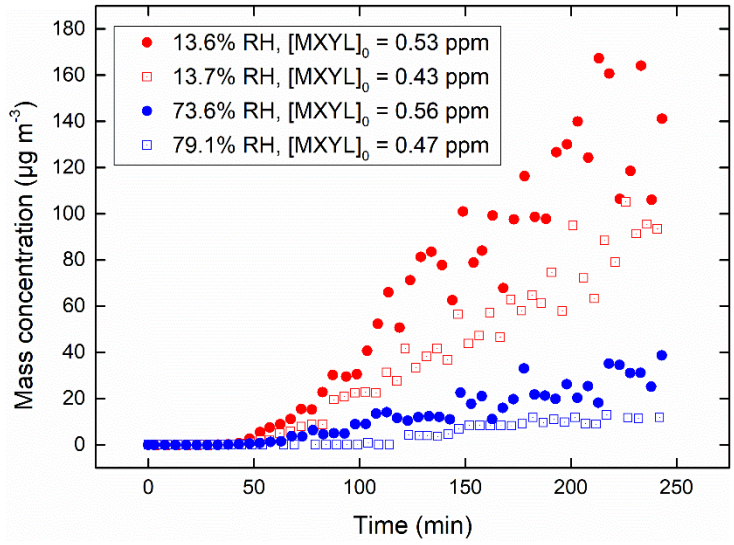

Figure 1. SOA mass concentrations as a function of irradiation time (corrected by particle wall loss).

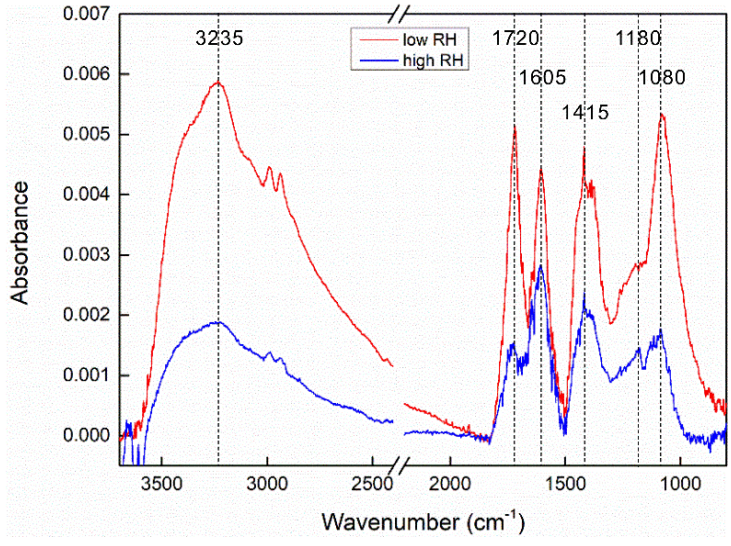

Figure 2. FTIR spectra of particles from photooxidation of *m*-xylene-OH experiments under low and high RH conditions.

Atmos. Chem. Phys. Discuss., https://doi.org/10.5194/acp-2019-20
Manuscript under review for journal Atmos. Chem. Phys.
Discussion started: 18 February 2019

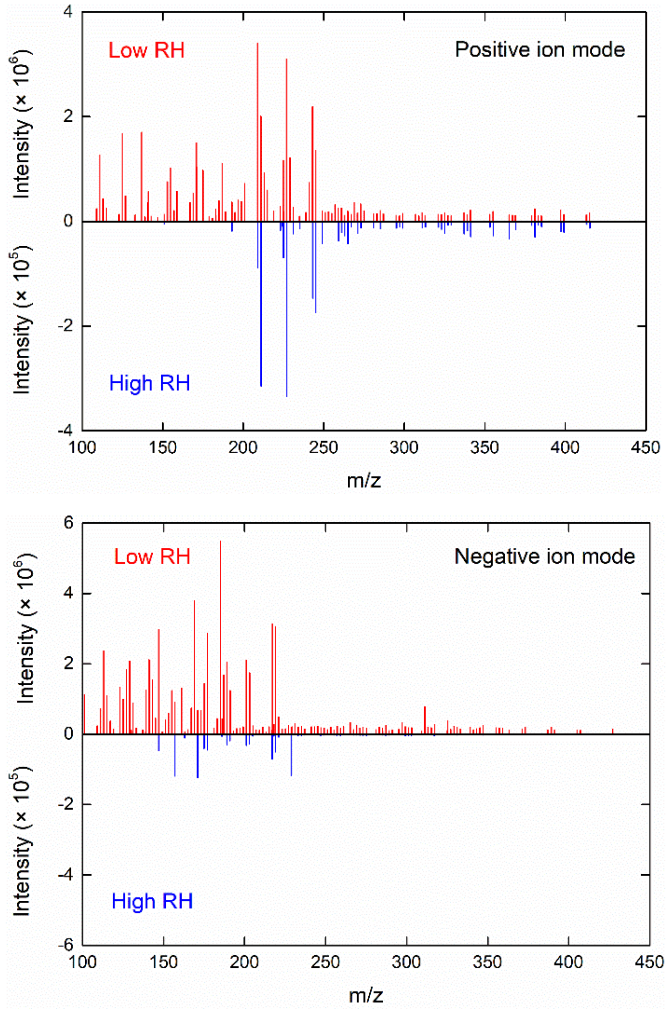

Figure 3. Selected background-subtraction HESI-Q Exactive-Orbitrap MS results of SOA in both positive and negative ion modes from the photooxidation of *m*-xylene-OH under both low and high RH conditions (Note that the Y-axis scales for low and high RH are largely different, 10^6 at low RH and 10^5 at high RH).

Atmos. Chem. Phys. Discuss., https://doi.org/10.5194/acp-2019-20
Manuscript under review for journal Atmos. Chem. Phys.
Discussion started: 18 February 2019

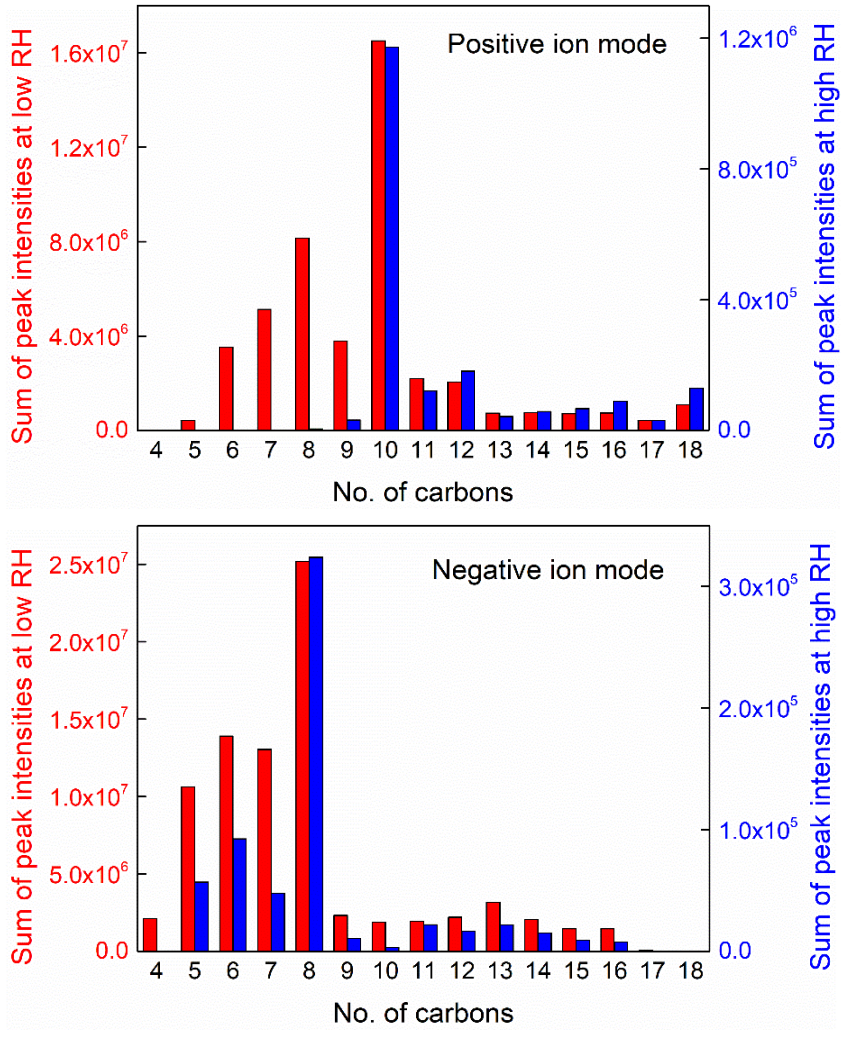

Figure 4. Sum of peak intensities based on peaks selected in Figure 3 as a function of the number of carbon atoms under the positive ion mode and negative ion mode (Note that the Y-axis scale at low and high RH are largely different, with a label step of 4.0×10^6 at low RH and 4.0×10^5 at high RH in the positive ion mode, 5.0×10^6 at low RH and 1.0×10^5 at high RH in the negative ion mode).

Atmos. Chem. Phys. Discuss., https://doi.org/10.5194/acp-2019-20
Manuscript under review for journal Atmos. Chem. Phys.
Discussion started: 18 February 2019

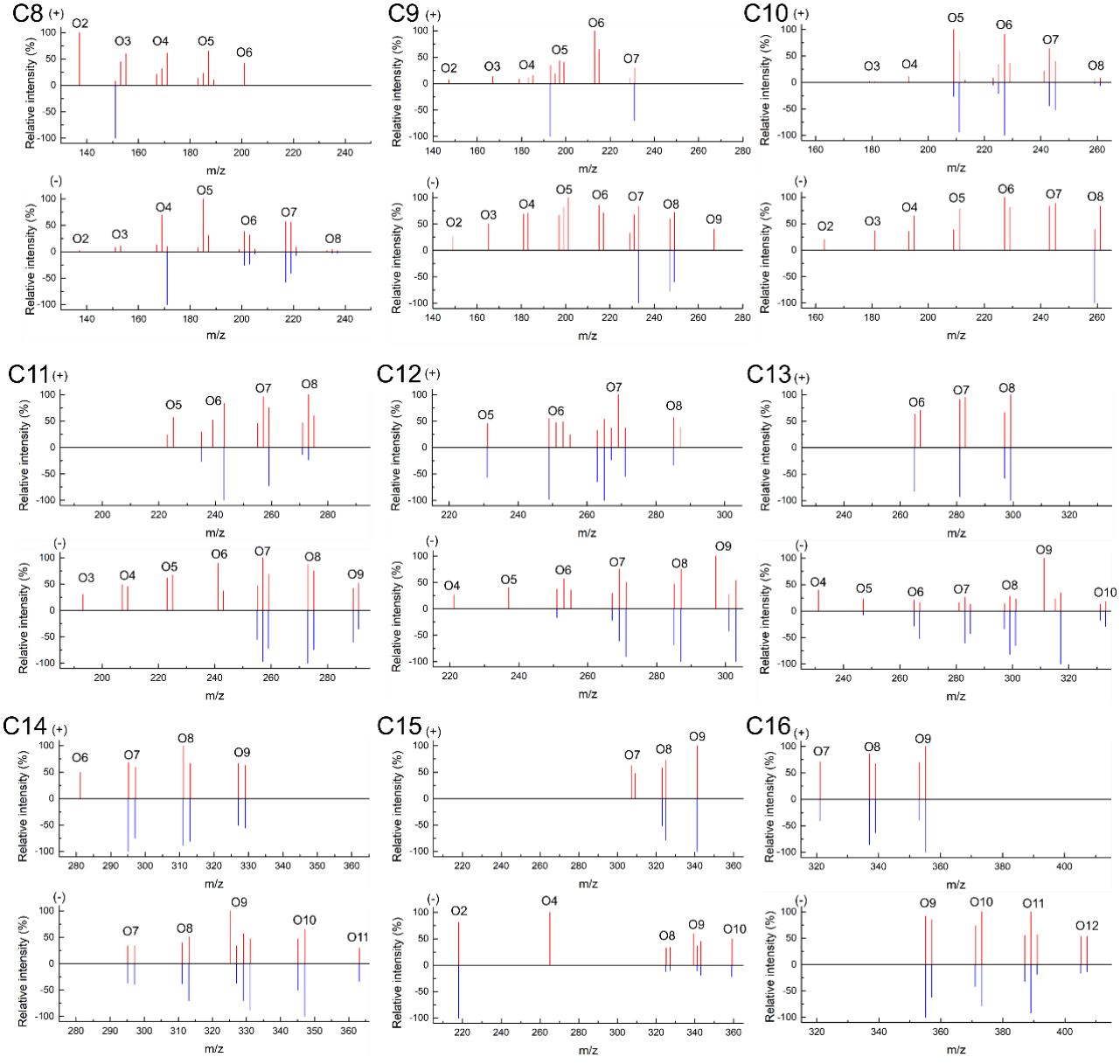

Figure 5. Mass spectra of SOA from *m*-xylene at both low (red) and high (blue) RH in the positive (+) and negative (-) ion modes, grouped with the same number of carbon atoms (from nC =8 to 16). On (n = 2, 3, ……, 12) means the number of oxygen atoms in the formula of the peak.

Atmos. Chem. Phys. Discuss., https://doi.org/10.5194/acp-2019-20
Manuscript under review for journal Atmos. Chem. Phys.
Discussion started: 18 February 2019

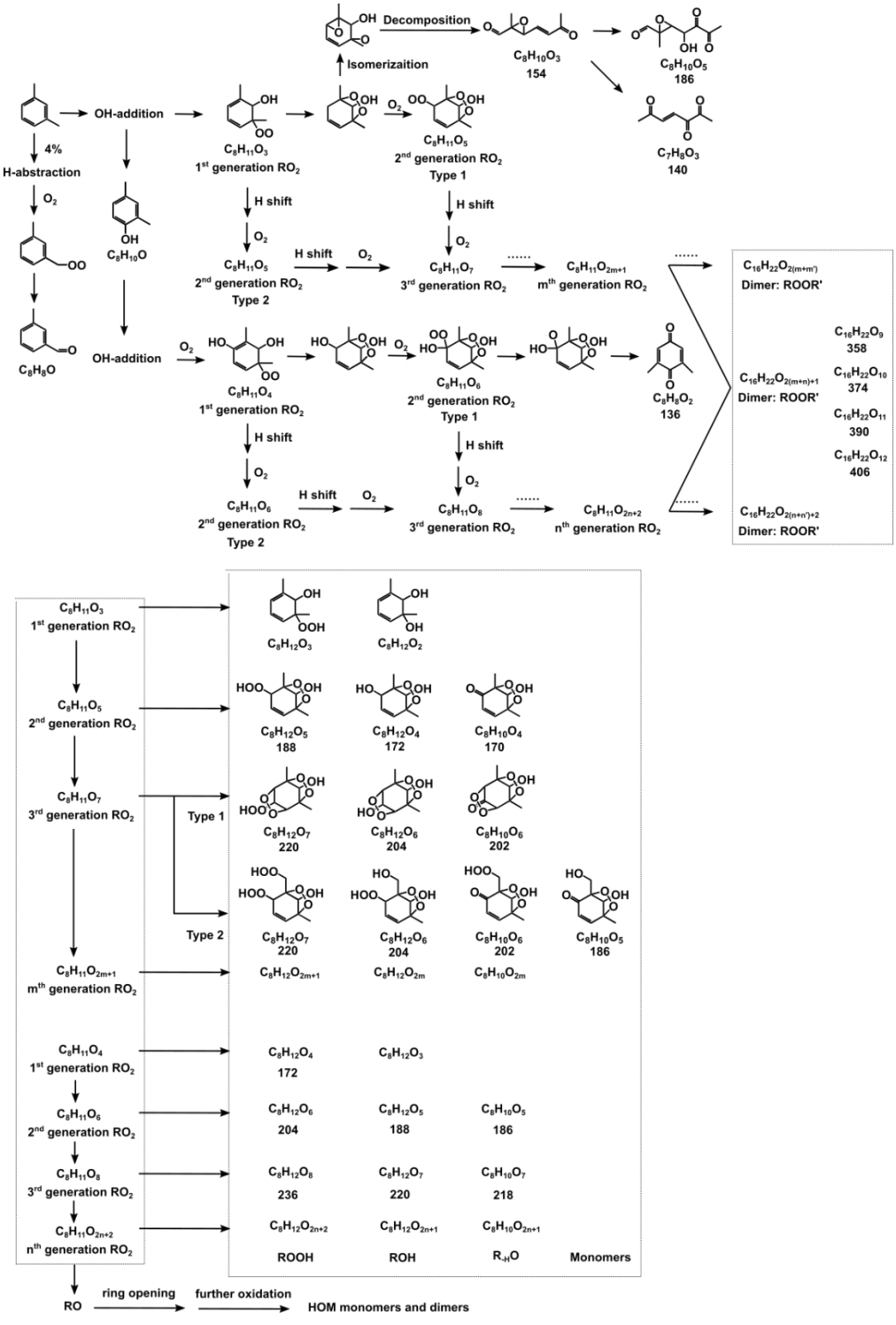

Scheme 1. The route of OH-initiated *m*-xylene oxidation. The number below the molecular formula is its molecular weight, which is determined by HRMS to exist in the particle phase.

Atmos. Chem. Phys. Discuss., https://doi.org/10.5194/acp-2019-20
Manuscript under review for journal Atmos. Chem. Phys.
Discussion started: 18 February 2019

Atmospheric Chemistry and Physics Discussions

Table 1. Experimental conditions, SOA concentrations and yields at the end of the experiments in *m*-xylene-OH oxidation system.

Exp. No.	[*m*-xylene]$_0$ (ppm)	RH (%)	T (°C)	[SOA]$_e$ (μg m^{-3})	SOA yield (%)
1	0.53	13.6	25.9	130.1	12.7
2	0.43	13.7	25.3	94.3	13.8
3	0.56	73.6	27.5	15.8	1.9
4	0.47	79.1	27.4	7.9	0.8

[SOA]$_e$ indicates the mass concentration of SOA at the end of each experiment with particle wall loss corrected.

Table 2. Absorbance positions of functional groups and the intensities at low and high RHs.

Absorption frequencies	Functionality	Intensity (× 10^{-3})		Ratio [a]
		low RH	high RH	
3235	O-H	5.9	1.9	0.32
1720	C=O	5.1	1.5	0.29
1605	COO^-, H_2O	4.4	2.8	0.64
1415	COO^-, CO-H	4.8	2.4	0.50
1180	C-O-C, C-O and OH of COOH	2.9	1.4	0.48
1080	C-C-OH	5.3	1.8	0.34

[a] Ratio of the intensity at high RH to that at low RH.

Atmos. Chem. Phys. Discuss., https://doi.org/10.5194/acp-2019-20
Manuscript under review for journal Atmos. Chem. Phys.
Discussion started: 18 February 2019

Atmospheric Chemistry and Physics Discussions

Table 3. Plausibility of different types of compounds with elemental formulae measured by HRMS in the positive ion mode.

Low RH	Measured (m/z)	137.05962	141.05445	155.07013	171.06509	187.06003
	Intensity	1.7×10^6	5.6×10^6	1.0×10^6	1.0×10^6	1.1×10^6
	Error (mDa)	0.6	1.3	1.2	1.2	1.2
High RH	Measured (m/z)	137.05931	141.05420	155.06985	171.06488	187.05678
	Intensity	1.4×10^5	-	-	-	-
	Error (mDa)	1.0	1.5	1.5	1.4	4.4
Ion formula		$[C_8H_9O_2]^+$	$[C_7H_9O_3]^+$	$[C_8H_{11}O_3]^+$	$[C_8H_{11}O_4]^+$	$[C_8H_{11}O_5]^+$
Proposed structure